Journal of the American College of Cardiology
© 2001 by the American College of Cardiology
Published by Elsevier Science Inc.

Vol. 38, No. 2, 2001
ISSN 0735-1097/01/$20.00
PII S0735-1097(01)01401-2

Characterization of the Anatomy and Conduction Velocities of the Human Right Atrial Flutter Circuit Determined by Noncontact Mapping

Richard J. Schilling, MD,* Nicholas S. Peters, MD,* Jeffrey Goldberger, MD,† Alan H. Kadish, MD,† D. Wyn Davies, MD*

London, United Kingdom, and Chicago, Illinois

OBJECTIVES This study was done to characterize human right atrial (RA) flutter (AFL) using noncontact mapping.

BACKGROUND Atrial flutter has been mapped using sequential techniques, but complex anatomy makes simultaneous global RA mapping difficult.

METHODS Noncontact mapping was used to map the RA of 13 patients with AFL (5 with previous attempts), 11 with counterclockwise and 2 with clockwise AFL. "Reconstructed" electrograms were validated against contact electrograms using cross-correlation. The Cartesian coordinates of points on a virtual endocardium were used to calculate the length and thus the conduction velocity (CV) of the AFL wave front within the tricuspid annulus-inferior vena cave isthmus (IS) and either side of the crista terminalis (CT).

RESULTS When clearly seen, the AFL wave front split (n = 3) or turned in the region of the coronary sinus os (n = 6). Activation progressed toward the tricuspid annulus (TA) from the surrounding RA in 10 patients, suggesting that the leading edge of the reentry wave front is not always at the TA. The IS length and CV was 47.73 ± 24.40 mm (mean ± SD) and 0.74 ± 0.36 m/s. The CV was similar for the smooth and trabeculated RA (1.16 ± 0.48 m/s and 1.22 ± 0.65 m/s, respectively [p = 0.67]) and faster than the IS (p = 0.03 and p = 0.05 for smooth and trabeculated, respectively).

CONCLUSIONS Noncontact mapping of AFL has been validated and has demonstrated that IS CV is significantly slower than either side of the CT. (J Am Coll Cardiol 2001;38:385–93) © 2001 by the American College of Cardiology

The mechanism for the majority of atrial flutter (AFL) has been well defined as a macroreentry circuit confined to the right atrium (RA) (1,2), which is dependent on the presence of anatomical obstacles and a line of block between the superior vena cava (SVC) and inferior vena cava (IVC) represented by the crista terminalis (CT), preventing the collision of posterior and anterior wave front. This line of block has been described as an anatomical structure that forms a functional barrier (3). The conduction velocity (CV) within the tricuspid annulus-inferior vena cava isthmus (IS) has also been noted to be slower in humans by some investigators (4,5) but not by others (6).

The hypothesis for this study was that AFL is the result of a macroreentry circuit that is not dependent on a complete line of block along the CT, nor on slowing of conduction within the IS.

METHODS

Patients. Patients with a history of AFL or both AFL and atrial fibrillation were studied.

From *St. Mary's Hospital and Imperial College School of Medicine, London, United Kingdom, and †Northwestern Memorial Hospital, Chicago, Illinois. This study was funded in part by the British Heart Foundation.

Manuscript received January 15, 2000; revised manuscript received March 1, 2001, accepted April 23, 2001.

Mapping procedure. The local ethics committees, whose guidelines were followed, approved the study. Quadripolar catheters were placed in the proximal CS, the high RA and right ventricular apex. A 7F deflectable mapping/ablation 4-mm tip catheter was advanced to the RA via the right femoral vein. Systemic arterial blood pressure was continuously monitored via a 6F femoral arterial sheath. A 9F sheath placed in the left femoral vein was used to introduce the noncontact mapping catheter. Contact catheter data and surface electrocardiograms (ECGs) were recorded simultaneously on a conventional electrophysiology system.

NONCONTACT MAPPING SYSTEM. The noncontact mapping system (EnSite 3000, Endocardial Solutions, St. Paul, Minnesota) has been described in detail elsewhere (7). Briefly, the system consists of a noncontact catheter (9F) with a multielectrode array (MEA) surrounding a 7.5-ml balloon mounted at the end. Raw data detected by the MEA is fed to a silicon graphics workstation via an amplifier.

Before deployment of the MEA, patients were given 10,000 IU heparin with boluses to maintain activated clotting time between 300 and 400 s throughout the study. The MEA catheter was deployed over a 0.035-in. (0.0889 cm) J-tipped guide wire advanced either to the SVC (n = 7) or the pulmonary outflow tract (n = 6), having been positioned using a 7F multipurpose catheter (Fig. 1). This

JACC Vol. 38, No. 2, 2001
August 2001:385–93

Abbreviations and Acronyms

AFL = atrial flutter
ASD = atrial septal defect
CI = confidence interval
CS = coronary sinus
CT = crista terminalis
CV = conduction velocity
ECG = electrocardiograms
IS = tricuspid annulus-inferior vena cava isthmus
IVC = inferior vena cava
LAO = left anterior oblique
MEA = multielectrode array
RA = right atrium/atrial
SVC = superior vena cava
TA = tricuspid annulus

was done to cant the balloon toward an area of interest (the atrioventricular junction), as previous data have demonstrated that the accuracy of electrogram reconstruction is greater with increasing proximity to the endocardium (7).

CATHETER LOCATION. The system locates any catheter with respect to the MEA using a "locator" signal, which serves two purposes. It is used to construct a three-dimensional computer model of the endocardium (virtual endocardium) providing a geometry matrix for the inverse solution. Geometric points are sampled at the beginning of the study during sinus rhythm or arrhythmia by gating 6 ms before the R-wave of the ECG during sinus rhythm or without gating during arrhythmia. The locator signal is also used to display and log the position of the catheter on the virtual endocardium and allows marking of anatomical locations identified using fluoroscopy and electrogram characteristics.

RECONSTRUCTION OF ELECTROGRAMS. The electrical activity detected by the electrodes on the MEA is generated primarily by the potential field on the endocardial surface. Using techniques to resolve these potentials, the system is able to reconstruct >3,000 unipolar electrograms simultaneously and superimpose them onto the virtual endocardium, producing isopotential maps (Fig. 2) with a color range representing voltage. Reconstructed electrograms can also be selected from sites on the virtual endocardium and displayed individually.

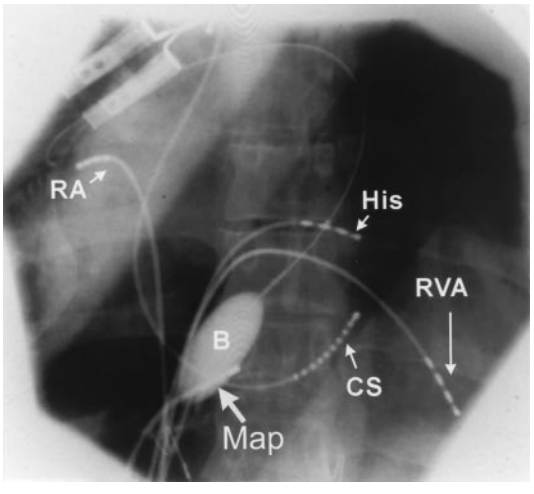

Figure 1. A posterio-anterior radiograph showing the multielectrode array (B) canted toward the tricupsid annulus by a guide wire passed out through the right ventricular outflow tract, so that the multielectrode array pigtail is straightened in the ventricle. Also seen are catheters in the high right atrium (RA), right ventricular apex (RVA), His bundle (His), coronary sinus (CS) and a mapping/ablation catheter on the tricupsid annulus-inferior vena cava isthmus (Map).

Mapping protocol. Baseline rhythm was recorded. The mapping catheter was then moved around the RA while fluoroscopy, electrograms and the locator signal were used to mark the following positions on the virtual endocardium: SVC; RA appendage; His bundle; coronary sinus (CS); IVC; six widely separated points around the tricuspid annulus (TA); IS. An electrophysiological study was then performed, and if the patient was in sinus rhythm, AFL was induced with RA stimulation. Once AFL had been induced and recorded, radiofrequency energy was applied to create a line of block in the IS. The appearance of AFL activation maps were validated by detailed examination of individual reconstructed electrograms.

Validation of electrogram reconstruction. Accuracy of electrogram reconstruction was assessed by cross-correlation between reconstructed and contact electrograms from the same endocardial location (7).

Distance and conduction velocity measurements. The noncontact system displays the Cartesian coordinates relative to the MEA center (in mm) of points on the virtual endocardium (8). It is therefore possible to derive straight-line distances between two points with the formula:

$$D = \sqrt{(x_1 - x_2)^2 + (y_1 - y_2)^2 + (z_1 - z_2)^2}$$

where x_1, y_1, z_1 and x_2, y_2, z_2 are the Cartesian coordinates of the two points and D is the straight-line distance between the points. This was used to calculate a series of short straight-line distances (<5 mm, to minimize the error caused by endocardial curvature) along the passage of the AFL wave front to obtain the total wave front distance. The time taken for the wave front to pass across a distance was determined by observing passage of the leading edge of the wave front on the isopotential map and confirmed by the time interval between the maximum −ve dV/dt of electrograms at the start and end of the distance measured. Conduction velocity was calculated from distance/time. The AFL wave front CV was calculated only in regions where the direction and path of the leading edge of the wave front could be clearly defined so that CV measurements were only made in directions parallel to wave front propagation, either side of the CT, and within the IS.

Definitions. ANATOMICAL TERMINOLOGY. Anatomical nomenclature was used that reflected the true orientation and positioning of the human heart in the thorax. Using this format the SVC and RA appendage are superior and the IVC and the IS are inferior to the TA. The His bundle is positioned in the posterosuperior aspect of the TA, the CS

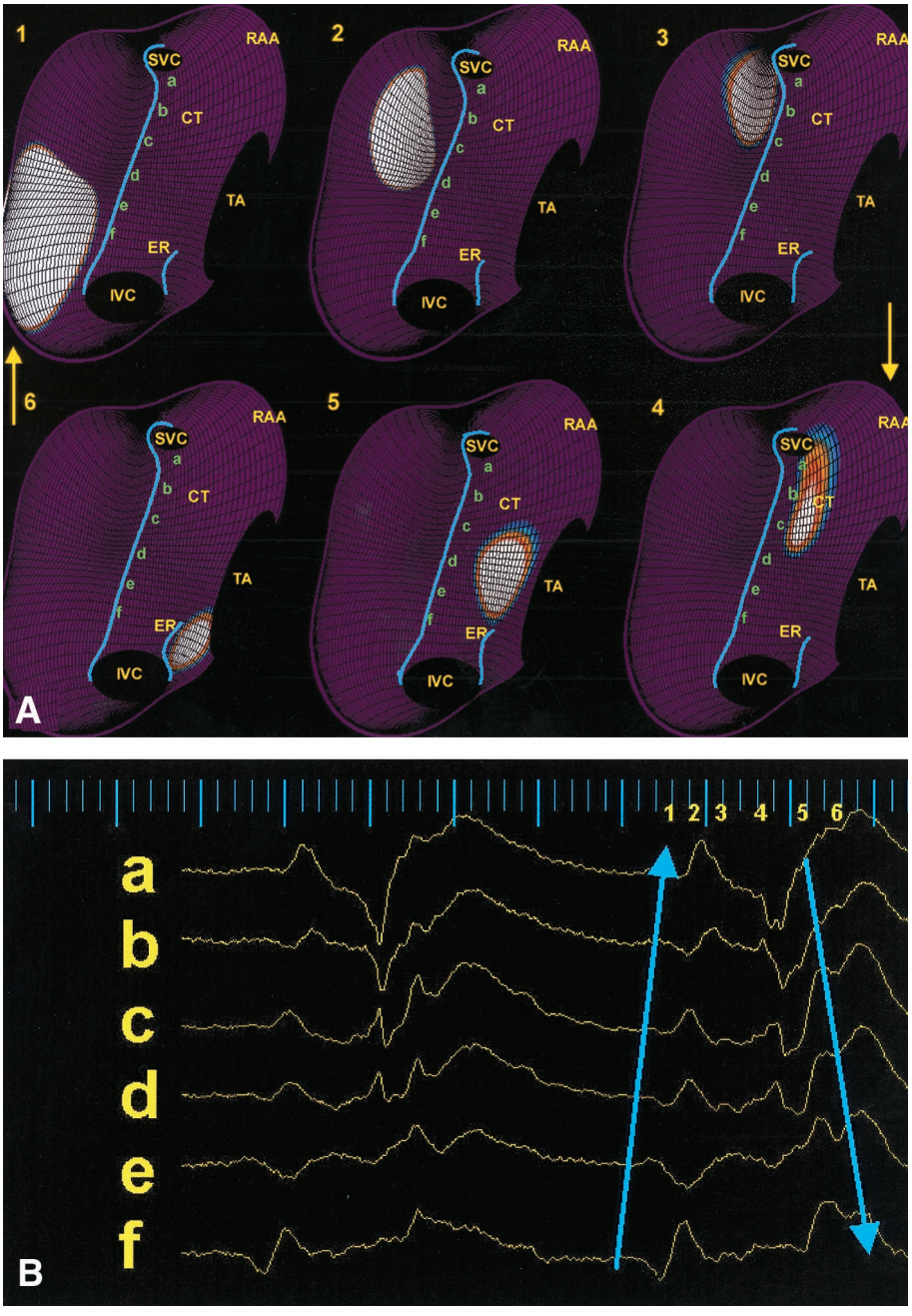

Figure 2. **(A)** Unipolar isopotential maps recorded from the right atrium (RA) during clockwise atrial flutter. The virtual endocardium has been cut and unfolded along the anterior border of the tricupsid annulus (TA), and the two edges are in continuity from top to bottom showing the concave inside surface of the endocardium. Even when this "open view" of the RA is shown, the system attempts to provide some perspective, and the virtual endocardium has been turned so that the lateral RA wall is seen in detail while the septum and isthmus are foreshortened. Anatomical locations have been identified using fluoroscopy and contact electrograms and marked in yellow on the virtual endocardium as follows: SVC = superior vena cava; IVC = inferior vena cava. The **blue lines** drawn on the lateral wall and above the CS os represent the probable position of the crista terminalis (CT) and eustachian ridge (ER) as defined by lines of conduction block to wave front propagation. The voltage range displayed on the isopotential map has been narrowed so that the map becomes equivalent to an activation map with unipolar activation (negative voltage) displayed as a colored region. Activation is validated by examination of individual electrograms, thus ensuring that noise artefact is excluded. The positions of the reconstructed bipolar electrograms (displayed in **A**) are labeled *a* to *f* from superior to inferior along the **blue line**, indicating a line of conduction block and the possible position of the CT. Activation is displayed on the virtual endocardium as a white and colored area. Activation **(white and colored region)** is seen progressing from the anterolateral RA near the IVC **(frame 1)** to the superior anterolateral RA **(frames 2 and 3)** along a line of block. Activation then turns at the SVC and progresses down the opposite side of the line of block from superior to inferior **(frames 3 to 5)** before it reaches the IS. Activation progresses through the IS **(frame 6 to 1)**, before activation of the anterolateral RA occurs again **(frame 1)**. **(B)** Reconstructed bipolar electrograms during two atrial flutter cycles are shown, from positions *a* to *f* along a line of block as shown in **B**. The numbers 1 to 6 indicate the time point from where the isopotential maps **(A)** were taken. Electrograms show double potentials with the isoelectric interval increasing from *a* to *f*. The long interval between the second potential on electrogram *f* and the first potential on the subsequent electrogram reflects the time for activation to pass through the IS.

in the posteroinferior aspect of the TA, and the CT is located in the lateral wall of the RA and is oriented from superior to inferior (9).

AFL. Atrial flutter was defined as a rapid atrial rate (>200 beats/min) characterized by a constant cycle length, polarity, morphology and amplitude of the recorded bipolar electrograms and as the presence of a single constant macroreentrant circuit with a constant atrial activation sequence (10). Cycle length was determined from unipolar reconstructed electrogram intervals and confirmed using contact electrograms.

IS. The tricuspid annulus-inferior vena cava isthmus was defined by anatomical landmarks identified using fluoroscopy and electrograms and was considered to extend from the CS posteriorly, the TA superiorly, and the IVC inferiorly. The anterior border of the IS was considered as a line joining the anteroinferior border of the TA with the anterior border of the IVC. It was further defined electrophysiologically by the demonstration of a distinct narrowing and expansion of the AFL wave front on isopotential maps as it entered and exited the IS.

DOUBLE POTENTIALS. These were defined as bipolar atrial electrograms with two discrete potentials per complete reentry circuit separated by either an isoelectric baseline or a low amplitude interval (11). When fractionated and double potentials were observed, local activation was considered to have occurred at the timing of the electrogram component with the largest negative deflection.

Statistics. Data are presented as means, SD and 95% confidence intervals (CI). Means of continuous, normally distributed data were compared using the Student *t* test.

RESULTS

Patients. Thirteen patients, 11 men, with a mean age of 60 years (range 33 to 75 years) (Table 1) were studied, 7 of whom were on amiodarone. Twelve were on other antiarrhythmic therapy, which was stopped at least five half-lives prior to study. Subsequent to mapping, 12 patients underwent radiofrequency ablation. One patient with predominantly atrial fibrillation had no ablation.

Three patients had atrial septal defects (ASDs) repaired (with no AFL before surgery) and two patients had idiopathic dilated cardiomyopathy. Five had had previous attempts at radiofrequency ablations of AFL and five were in AFL at the start of the procedure. No patient suffered a complication as a result of the mapping procedures.

AFL. Mean AFL cycle length was 240.92 ± 35.45 ms, with no difference between reconstructed and contact electrogram measurements. All 13 patients had IS-dependent counterclockwise (n = 11) or clockwise (n = 2) AFL. In none of the patients with prior ASD repair was the ASD patch used as a barrier defining the AFL circuit. Apart from the direction, the AFL circuit and CV did not differ

Table 1. Patient Results

Patient	RADD/ RAL	ECG	Map	Proc Time	Fluoro Time	TA Act	IS L (mm)	IS Start	IS End	CS	IS CV (m/s)	Smooth CV (m/s)	Trab CV (m/s)	Exit Morph	Time in IS
1‡	4.2/5.1	−ve	C	375	61.7	To	42.59	6'00"	4'30"	4'15"	0.54	1.23	1.25	Splits at entry	12% (30/241)
2‡	5.7/6.5	−ve	AC	510	99.9	Unseen	40.37	6'30"	4'30"	4'00"	0.65	n/a	n/a	Turns	48% (119/246)
3	4.4/5	−ve	AC	455	106.4	To	53.06	5'30"	4'30"	4'00"	1.70	1.73	1.70	Splits	21% (46/214)
4†	6/8	−ve	AC	195	54.1	Away	112.11	6'00"	4'30"	4'00"	0.93	1.19	2.20	Inferior exit	54% (154/285)
5*	4.5/6.5	−ve	AC	210	68.1	To	49.69	5'30"	4'00"	4'00"	0.87	0.53	0.33	Turns	31% (81/261)
6	5.3/6.7	−ve	AC	215	59	Away	40.53	6'30"	5'30"	4'00"	0.61	0.52	0.47	Inferior exit	25% (40/160)
7*	4.2/5.8	−ve	AC	280	74.9	To	73.53	6'30"	4'30"	4'15"	0.71	1.98	1.87	Turns	27% (62/231)
8	5.3/9.5	+ve	C	450	76	To	36.68	6'30"	4'30"	4'00"	0.68	1.04	0.90	Turns at entry	26% (54/210)
9	3.6/7.2	−ve	AC	360	84	To	25.39	6'30"	4'30"	4'00"	0.82	0.63	0.83	Turns	14% (31/229)
10	4.3/7	−ve	AC	370	73	To	46.67	6'30"	4'00"	3'30"	0.34	1.45	2.09	Splits	43% (119/280)
11	5/8.3	−ve	AC	280	101	To	23.22	6'30"	4'30"	3'00"	0.31	1.01	1.15	Not clearly seen	27% (73/274)
12*	2.8/6	Biphasic	AC	270	65	To	28.95	5'30"	4'00"	3'30"	0.72	1.48	0.67	Turns	15% (40/260)
13	5.1/10	−ve	AC	500	94	To	n/a	n/a	n/a	n/a	n/a	n/a	n/a	Turns	Not clearly seen
Mean	4.7/7.1			343.85	78.24		47.73				0.74	1.16	1.22		
SD	0.9/1.6			110.98	17.34		24.40				0.36	0.48	0.65		

*Previous RF; †previous ASD; ‡previous ASD repair and RF.
ASD = atrial septal defect; CS = the position of the CS on this clock face; ECG = the morphology of the P-waves in the inferior ECG leads; Exit Morph = the wave front morphology as it exits the IS; Fluoro time = fluoroscopy time (mins); IS L = IS length; IS start = IS start as determined using a clock face (see text for details); Map = direction of AFL wave front on conventional and noncontact mapping (these correlated in all); Proc Time = procedure time (mins); RADD = RA diastolic diameter measured from the septum to the anterior wall (cm); RAL = RA length measured from the lateral wall to the TA (cm); RF = radiofrequency; Smooth CV = RA CV at the smooth side of the CT; TA Act = the direction of RA activation with reference to the TA as seen on noncontact mapping; Time in IS = percentage of time the wave front spent in the IS (time in isthmus [ms]/time in rest of RA [ms]); Trab CV = RA CV at the trabeculated side of the CT.

significantly between the patients with clockwise and counterclockwise AFL.

VALIDATION OF ELECTROGRAM RECONSTRUCTION DURING AFL. Cross-correlation of reconstructed and contact AFL electrograms recorded at 127 different locations was 0.73 ± 0.18 for all distances and 0.8 ± 0.11 for the 62 locations <35 mm from the center of the MEA ($p < 0.001$), a phenomenon described before (7). Timing difference between contact and reconstructed electrograms was 7.9 ± 12.1 ms for all locations and 3.9 ± 3.7 for those <35 mm from the MEA ($p < 0.001$).

CHARACTERISTICS OF IS ACTIVATION. The AFL wave front was seen throughout the entire IS in nine patients with some signal attenuation in three patients with previous ablation procedures. In one patient signal attenuation prevented the IS being clearly defined electrophysiologically. In the remaining patients the IS extent was described using a clock-face projected onto the TA while viewed in the left anterior oblique (LAO) projection. The IS length was seen to extend from 4 h 30 min to 6 h 30 min with expansion/narrowing of the wave front being distant from the CS, which most commonly positioned at 4 o'clock (Table 1). In three patients the wave front was seen to split as it passed the CS and the region of the eustachian ridge, one wave front passing inferiorly and one superiorly to the CS before fusing again. In seven patients a single activation wave front slowed and turned superiorly toward the TA in the region of the CS and eustachian ridge, and in two patients the wave front slowed and emerged from the IS inferiorly, suggesting some variation of conduction properties in the posterior IS.

LATERAL WALL ACTIVATION PATTERNS DURING AFL. A line of block was seen on the posterolateral RA wall in 12 patients during AFL. This was confirmed by the presence of double potentials in electrograms reconstructed along this line (Fig. 2A,B). In 10 patients the line of block extended from the IVC to the SVC. In one patient the line of block extended superiorly from the IVC to the mid-lateral RA but did not reach the SVC. In one patient the line of block extended from the SVC to the low RA, but slow activation was seen progressing over a 70-ms interval between the IVC and the CT, which was confirmed by fractionated, reconstructed electrograms of similar duration (Fig. 3A,B).

ACTIVATION AROUND THE TA. The pattern of AFL activation wave front in relation to the portions of the TA not adjacent to the IS (non-IS TA) and at the superior turnaround was seen in 12 patients. The AFL activation progressed along the CT and then spread toward the non-IS TA in 10 patients (Fig. 4). Specifically, as the wave front passed in front of the SVC and through the RA appendage the portion of the wave front closest to the CT progressed more rapidly than that adjacent to the TA, which meant that the RA surrounding the TA was activated almost simultaneously by activation progressing from the CT.

CONDUCTION VELOCITY WITHIN THE AFL CIRCUIT. Passage of the AFL wave front through the IS took 70.75 ± 40.22 ms (95% CI 47.99 to 93.51 ms) and occupied 28.58 ± 13.45% of the AFL cycle length. When all patients, including those with prior ablation, were studied, the CV in the IS (0.74 ± 0.36 m/s [95% CI 0.54 to 0.944 m/s]) was slightly lower than in the smooth RA, posterior to the CT (1.16 ± 0.48 m/s [95% CI 0.88 to 1.45 m/s]) ($p = 0.03$) or the trabeculated RA, anterior to the CT (1.22 ± 0.65 m/s) ($p = 0.05$). However, when the five patients with prior RF were excluded, the mean RA CV was slightly lower, but the difference was not statistically significant. The CVs were 0.77 ± 0.47 m/s for the IS, 1.08 ± 0.43 m/s for smooth RA and IS CV, and 1.33 ± 0.67 m/s for trabeculated RA ($p = 0.13$ and $p = 0.09$, respectively).

DISCUSSION

Noncontact mapping produced high-resolution maps of the entire AFL circuit in the intact human RA for the first time. The maps demonstrated macroreentry during AFL and showed functional and anatomical variations in circuits between patients. Noncontact mapping also allowed calculation of CV of the AFL circuit.

Validation of noncontact mapping. Electrogram reconstruction using noncontact mapping has been validated in the human ventricle during sinus rhythm (7) and ventricular tachycardia (12) and the RA during atrial fibrillation (13). This is the first validation of AFL, and the results are similar to those during atrial fibrillation.

Location of the re-entry circuit in AFL. The majority of the AFLs are caused by a macrore-entry circuit confined to the RA, which is dependent on anatomical obstacles within the RA (1,14). Previous investigators have concluded that AFL may (4,5) or may not (6) be dependent on slow conduction in the IS. The inferior turning point has been identified as the IS (2,3,15), and the upper turning point is located either anterior or posterior to the SVC (4,16). It has also been suggested that the re-entry wave front producing counterclockwise AFL in the RA rotates around the TA, with the TA constituting the anterior continuous barrier around which the wave front rotates (17), with activation of the rest of the RA radiating from the TA.

The noncontact mapping system has produced high-resolution maps of the entire AFL circuit using data acquired simultaneously. The majority of the AFLs described here are consistent with previous observations that the TA and CT serve as continuous barriers to conduction, but several new observations have been made. First, the leading edge of activation is usually not directly around the TA. In addition, one of the RAs mapped during AFL had a break in the line of block in the CT, demonstrating that it is not always a continuous line of block.

The role of the CT. The presence of double potentials (3,18) during AFL has suggested the presence of barriers to conduction (11,19) in the lateral RA, and it has been

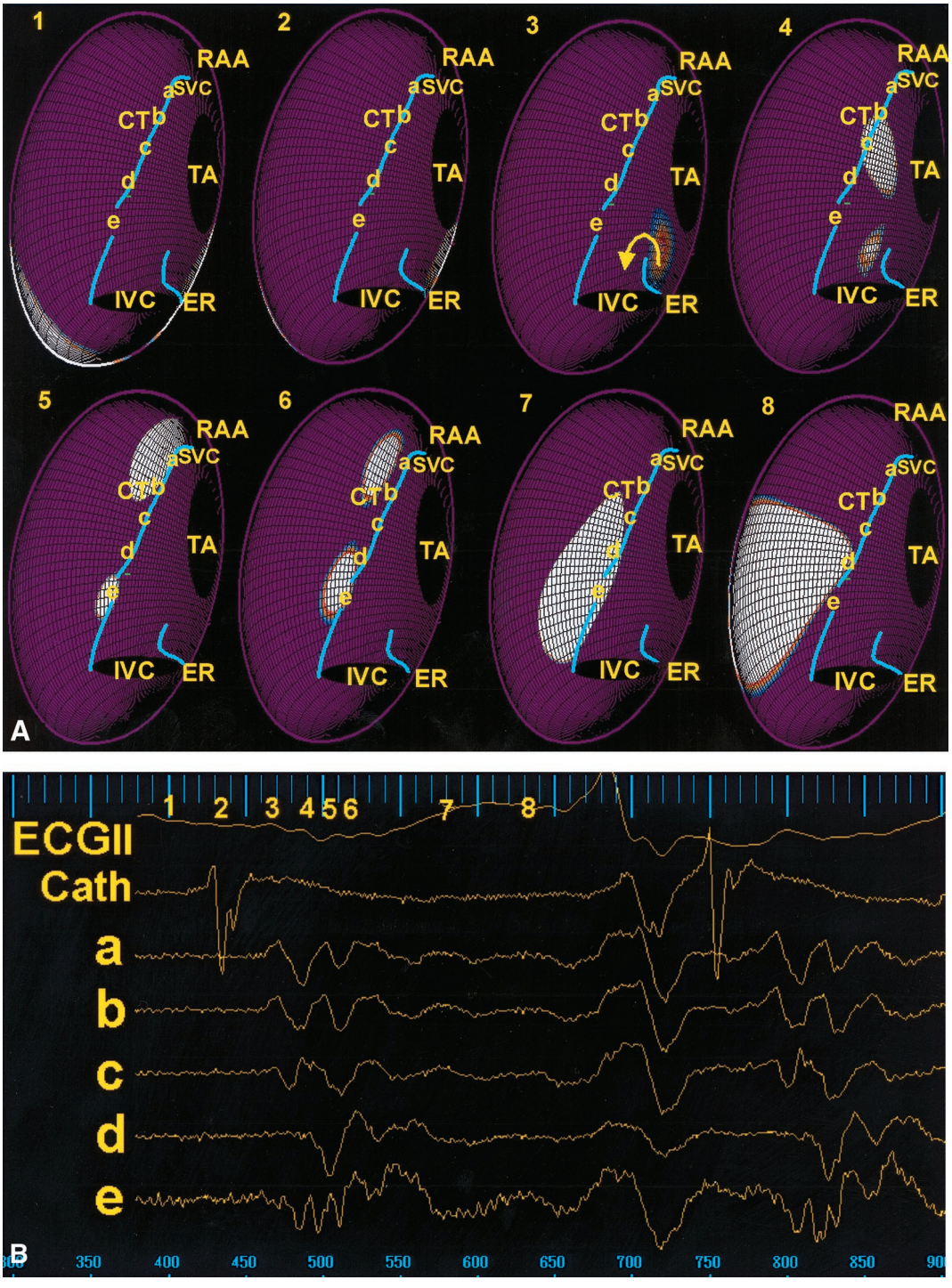

Figure 3. **(A)** Unipolar isopotential maps recorded during counterclockwise atrial fluter. The endocardium is opened, unfolded and flattened, resulting in stretching of the anterolateral right atrium (RA) **(spread grid-lines)** and compression of the posteroseptal wall **(packed grid-lines)**. The positions at which bipolar electrograms have been reconstructed and displayed in **B** are labeled as *a* to *e* from superior to inferior along a line of block, compatible with the position of the crista terminalis (CT). Activation passes through the tricupsid annulus-inferior vena cava isthmus **(frame 1)** and turns toward the tricuspid annulus (TA) **(arrow)** around a line of block (possibly the eustachian ridge [ER]) **(frame 2)**. The wave front the then begins to split **(frame 3)** with one front moving superiorly along the line of block while the second front moves slowly along the ER. The first wave front turns at the superior vena cava (SVC) **(frame 4)** and then passes inferiorly along the line of block **(frames 5 and 6)**. The second front passes slowly through a break in the line of block **(frames 4 to 6)**. The first and second wave fronts then fuse **(frame 7)**, pass around the inferior vena cava (IVC) to enter **(frame 8)** and pass through the IS **(frame 1)**. **(B)** The surface electrocardiographic lead II, an electrogram from a catheter at the coronary sinus os and reconstructed bipolar electrograms from points *a* to *e* on the isopotential maps in **A**. The numbers 1 to 8 represent the points at which the isopotential maps have been displayed in **A**. The electrograms from the line of block show double potentials apart from those recorded at the break in the line of block, which are long and fractionated, representing the slow activation at this point.

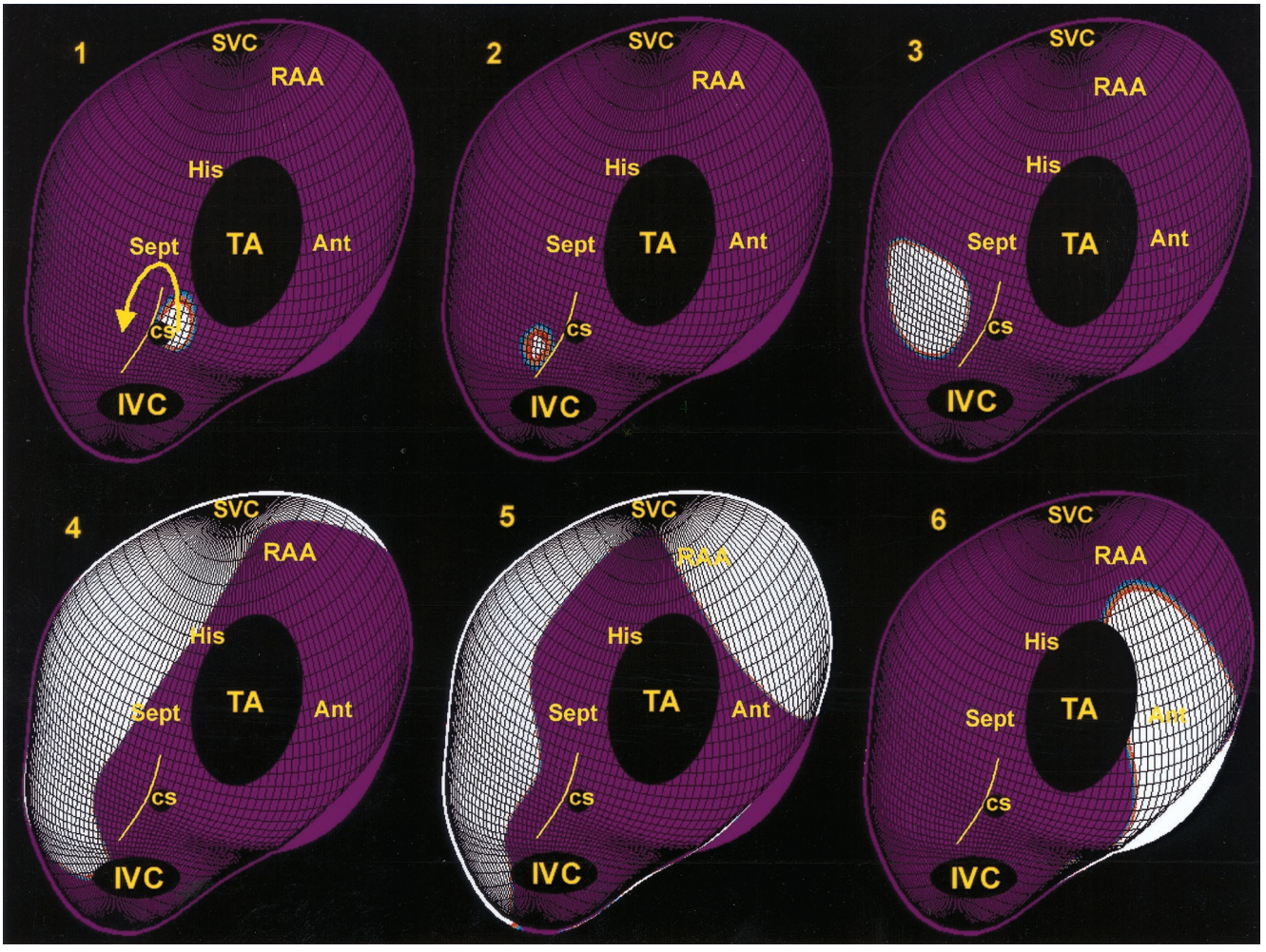

Figure 4. Isopotential maps with the lateral wall of the right atrium (RA) removed so that the virtual endocardium shows the septum (Sept), tricuspid annulus-inferior vena cava (IVC) isthmus (IS) and tricuspid annulus (TA) in detail and the reader is looking in toward the TA. The possible position of the eustachian ridge is drawn onto the virtual endocardium as a yellow line. The atrial flutter wave front enters and passes through the IS **(frame 1)** and encounters a line of block at the posterior IS. The wave front turns toward the TA **(arrow)**, passes up over this line of block and back down the posterior aspect of the line of block **(frames 2 and 3)**. The wave front exits the IS and activates the posterior RA **(frames 3 to 4)**. The posterolateral RA activates before the TA as does the anterior RA **(frames 4 to 6)**. Activation then progresses from both areas toward the TA where the wave front(s) extinguish. The anterolateral wave front then passes into the anterior IS and through the IS to repeat the circuit **(frame 6 to 1)**. Ant - anterior; cs = coronary sinus; His = His bundle; SVC = superior vena cava.

inferred that these may be the center of the AFL re-entry circuit (3). Intracardiac echocardiography has confirmed that these electrical barriers are related to the structures of the CT and the eustachian ridge (3), but the nature of the conduction block in these regions has not been clearly defined; it has been postulated that the presence of conduction block differentiates between patients with and without AFL.

Noncontact mapping during AFL has confirmed the presence of a line of conduction block in the lateral RA that is compatible with the location of the CT with both double potentials on reconstructed electrograms in this region and demonstration of conduction block on isopotential maps. Noncontact mapping has demonstrated that this line of conduction block is not complete in all patients during AFL. The AFL wave front has been seen to turn from the posteroseptal RA to the anterolateral RA at the level of the midlateral RA in one patient. In another patient the main wave front was seen to split, with one daughter wave front turning at the level of the IVC with the slow conduction of the wave front through this region preventing premature activation and termination of the re-entry circuit.

Lower-loop re-entry has already been described by Shah et al. (5) and Cheng et al. (20,21) using recordings acquired from catheter electrode recordings taken from the TA and septum. They were unable to distinguish between lower-loop re-entry and a focal atrial tachycardia located at the inferior-anterior aspect of the RA, but they made the point that lower-loop re-entry was noninducible after IS ablation, and it seemed reasonable to assume that this rhythm was isthmus dependent. Cheng et al. also concede that they had insufficient sites, and specifically no data recorded from the posterior RA. Larger numbers of electrograms allowed us to confirm the deductions made

by Cheng et al. that the AFL wave front can pass through the inferior CT.

Activation in the region of the CS os. The region of the triangle of Koch and posterior IS has complex anatomy, comprised in part by the eustachian ridge extending into the tendon of Todaro and the CS. Intraoperative mapping in one case of common AFL has revealed slow conduction between the CS and the tricuspid valve colliding with another wave front of activation traveling between the CS and the IVC (22). Slow and irregular activation seen in Koch's triangle may be due to fiber arrangement (23), and it has also been noted that circumferential fibers found around the rest of the TA may be absent in this area (24). Noncontact mapping demonstrated that the wave front slows and turns in the posterior region of the triangle of Koch in the majority of patients, suggesting that it encounters a line of block at the site of the eustachian ridge. Splitting of the wave fronts in this region was also seen, and this may have been a feature of the wave front passing around the CS os. Alternatively, part of the activation wave front may have passed under the eustachian ridge, becoming intramural and thus not visible to the noncontact system. Only two patients with clockwise AFL were included in this series, but a similar activation pattern was seen in the region of the eustachian ridge in these patients, indicating that this is not specific to activation of the wave front direction.

Conduction velocity within the IS. The mean CV of the AFL wave front within the IS was slower than smooth and trabeculated RA adjacent to the CT but only when patients with previous radiofrequency were included in the analysis. This may indicate that IS conduction is not slower than the rest of the RA unless the patient has had previous radiofrequency to the IS; however, the patient numbers studied were small, and this cannot therefore be substantiated by this study, but it is consistent with previous studies. Kinder et al. (6) concluded that there is no functional slowing of conduction within the IS during AFL compared with sinus rhythm, but CV was not measured and comparison with the rest of the atrium was not performed. Tai et al. (4) measured IS CV during pacing (but not AFL) by dividing the bipolar electrogram intervals by interelectrode spacing and found that IS CVs were lower than in our study (0.336 ± 0.045 m/s) and were lower in the mid IS compared with the lateral IS. This may be explained because distance traveled across a complex curved surface is likely to be underestimated by the distance between electrodes on a straight catheter bridging this distance. Also, using bipolar electrograms makes clear definition of local activation difficult.

Study limitations. A proportion of the patients studied had been on amiodarone therapy, which may have affected CV; the results should thus be interpreted with caution. In measuring CV distance, measurements were calculated using a series of short straight-line distances that are an approximation of the true curved surface of the RA and are therefore subject to error. Calculating the shortest distance that a wave front travels is difficult on complex curved surfaces, which is why wave front CV was measured only in portions of the AFL circuit where passage of the leading edge was clearly defined (i.e., within the IS and on either side of the CT). The calculation of CV using contact arrays is also prone to these problems because it is calculated by measuring distances between electrodes on the arrays, which are clearly short straight-line distances. Also, acquisition of clear signals requires that pressure be used to achieve contact between the array and epicardium, which may distort the anatomy and affect the CV.

Conclusions. Using noncontact mapping we have produced the first high-resolution maps of the intact human RA during AFL. We confirm previous observations that the line of block represented by the CT is not necessarily complete in all patients. Maps of activation at the triangle of Koch explain why a line of block between the TA and CS os may terminate some cases of AFL because there is conduction block posteroinferior to the CS os possibly related to the eustachian ridge. The AFL wave front CV within the IS has been measured and confirmed that CV may be, but is not always, slower than the rest of the AFL circuit.

Reprint requests and correspondence: Dr. Richard Schilling, Waller Department of Cardiology, St. Mary's Hospital, Praed St., London W2 1NY, United Kingdom. E-mail: r.schilling@ic.ac.uk.

REFERENCES

1. Arenal A, Almendral J, Alday JM, et al. Rate-dependent conduction block of the crista terminalis in patients with typical atrial flutter influence on evaluation of cavotricuspid isthmus conduction block. Circulation 1999;99:2771–8.
2. Cosio F, Lopez-Gil M, Arribas F, Palacios J, Goicolea A, Nunez A. Mechanisms of entrainment of human common atrial flutter studied with multiple endocardial recordings. Circulation 1994;89:2117–25.
3. Olgin JE, Kalman JM, Fitzpatrick AP, Lesh MD. Role of right atrial endocardial structures as barriers to conduction during human type I atrial flutter. Activation and entrainment mapping guided by intracardiac echocardiography. Circulation 1995;92:1839–48.
4. Tai CT, Chen SA, Chiang CE, et al. Characterization of low right atrial isthmus as the slow conduction zone and pharmacological target in typical atrial flutter. Circulation 1997;96:2601–11.
5. Shah DC, Jaïs P, Haïssaguerre M, et al. Three-dimensional mapping of the common atrial flutter circuit in the right atrium. Circulation 1997;96:3904–12.
6. Kinder C, Kall J, Kopp D, Rubenstein D, Burke M, Wilber D. Conduction properties of the inferior vena cava-tricuspid annular isthmus in patients with typical atrial flutter. J Cardiovasc Electrophysiol 1997;8:727–37.
7. Schilling RJ, Peters NS, Davies DW. A non-contact catheter for simultaneous endocardial mapping in the human left ventricle: comparison of contact and reconstructed electrograms during sinus rhythm. Circulation 1998;98:887–98.
8. Schilling RJ, Davies DW, Peters NS. Characteristics of sinus rhythm electrograms at sites of ablation of ventricular tachycardia relative to all other sites: a non-contact mapping study of the entire left ventricle. J Cardiovasc Electrophysiol 1998;9:921–33.
9. Cosio FG, Anderson RH, Kuck KH, et al. Living anatomy of the atrioventricular junctions. A guide to electrophysiologic mapping: a consensus statement from the Cardiac Nomenclature Study Group, working group of arrhythmias, European Society of Cardiology, and the task force on cardiac nomenclature from NASPE. Circulation 1999;100:e31–7.
10. Ortiz J, Igarashi M, Gonzalez HX, Laurita K, Rudy Y, Waldo AL.

Mechanism of spontaneous termination of stable atrial flutter in the canine sterile pericarditis model. Circulation 1993;88:1866–77.
11. Olshansky B, Okumura K, Henthorn RW, Waldo AL. Characterization of double potentials in human atrial flutter. Studies during transient entrainment. J Am Coll Cardiol 1990;15:833–41.
12. Schilling RJ, Peters NS, Davies DW. Feasibility of a non-contact catheter for endocardial mapping of human ventricular tachycardia. Circulation 1999;99:2543–52.
13. Schilling RJ, Kadish AH, Peters NS, Goldberger J, Davies DW. Endocardial mapping of atrial fibrillation in the human right atrium using a non-contact catheter. Eur Heart J 2000;21:550–64.
14. Cosio FG, Lopez-Gil M, Goicolea A, Arribas F. Electrophysiologic studies in atrial flutter. Clin Cardiol 1992;15:667–73.
15. Cosio FG, Lopez-Gil M, Goicolea A, Arribas F, Barroso J. Radiofrequency ablation of the inferior vena cava-tricuspid valve isthmus in common atrial flutter. Am J Cardiol 1993;71:705–9.
16. Tsuchiya T, Okumura K, Tabuchi T, Iwasa A, Yasue H, Yamabe H. The upper turnover site in the reentry circuit of common atrial flutter. Am J Cardiol 1996;78:1439–42.
17. Kalman JM, Olgin JE, Saxon LA, Fisher WG, Lee RJ, Lesh MD. Activation and entrainment mapping defines the tricuspid annulus as the anterior barrier in typical atrial flutter. Circulation 1996;94:398–406.
18. Kalman JM, Olgin JE, Saxon LA, Lee RJ, Scheinman MM, Lesh MD. Electrocardiographic and electrophysiologic characterization of atypical atrial flutter in man: use of activation and entrainment mapping and implications for catheter ablation. J Cardiovasc Electrophysiol 1997;8:121–44.
19. Cosio FG, Arribas F, Barbero JM, Kallmeyer C, Goicolea A. Validation of double-spike electrograms as markers of conduction delay or block in atrial flutter. Am J Cardiol 1988;61:775–80.
20. Cheng J, Cabeen WR Jr, Scheinman MM. Right atrial flutter due to lower loop reentry: mechanism and anatomic substrates. Circulation 1999;99:1700–5.
21. Cheng J, Scheinman MM. Characteristics of double-wave reentry induced by programmed stimulation in patients with typical atrial flutter. Circulation 1998;97:1589–96.
22. Saumarez RC, Parker J, Camm J. Geometrically accurate mapping of the atrioventricular node region during surgery. J Am Coll Cardiol 1992;19:601–6.
23. Racker DK. Atrioventricular node and input pathways: a correlated gross anatomical and histological study of the canine atrioventricular junctional region. Anat Rec 1989;224:336–54.
24. Racker DK, Ursell PC, Hoffman BF. Anatomy of the tricuspid annulus: circumferential myofibers as the structural basis for atrial flutter in a canine model. Circulation 1991;84:841–51.